

Accepted Manuscript

Interface-induced controllable synthesis of Cu₂O nanocubes for electroreduction CO₂ to C₂H₄

Wenhang Wang, Hui Ning, Zhongxue Yang, Zhaoxuan Feng, Jialin Wang, Xiaoshan Wang, Qinhu Mao, Wenting Wu, Qingshan Zhao, Han Hu, Yan Song, Mingbo Wu

PII: S0013-4686(19)30569-9

DOI: <https://doi.org/10.1016/j.electacta.2019.03.146>

Reference: EA 33862

To appear in: *Electrochimica Acta*

Received Date: 29 November 2018

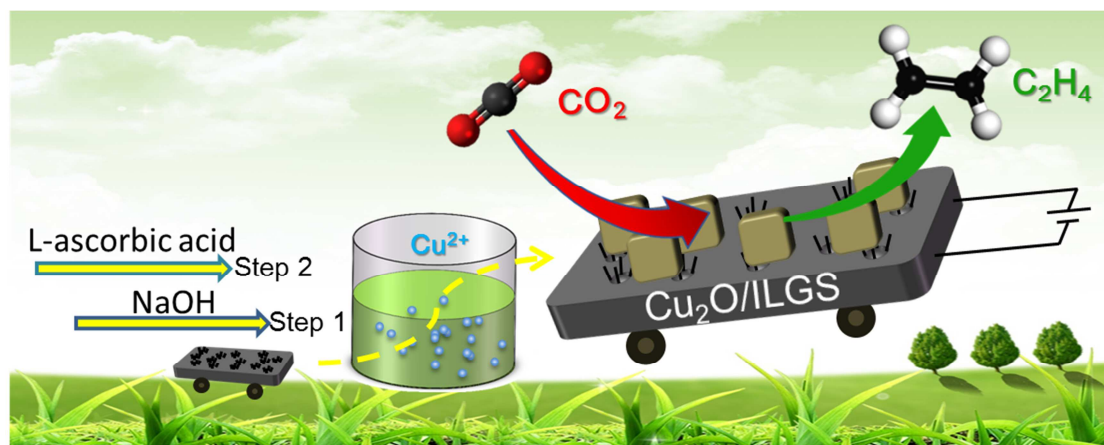
Revised Date: 12 March 2019

Accepted Date: 20 March 2019

Please cite this article as: W. Wang, H. Ning, Z. Yang, Z. Feng, J. Wang, X. Wang, Q. Mao, W. Wu, Q. Zhao, H. Hu, Y. Song, M. Wu, Interface-induced controllable synthesis of Cu₂O nanocubes for electroreduction CO₂ to C₂H₄, *Electrochimica Acta* (2019), doi: <https://doi.org/10.1016/j.electacta.2019.03.146>.

This is a PDF file of an unedited manuscript that has been accepted for publication. As a service to our customers we are providing this early version of the manuscript. The manuscript will undergo copyediting, typesetting, and review of the resulting proof before it is published in its final form. Please note that during the production process errors may be discovered which could affect the content, and all legal disclaimers that apply to the journal pertain.





Interface-induced controllable synthesis of Cu₂O nanocubes for electroreduction CO₂ to C₂H₄

Wenhang Wang^a, Hui Ning^{a,*}, Zhongxue Yang^a, Zhaoxuan Feng^a, Jialin Wang^a, Xiaoshan Wang^a,
Qinhu Mao^a, Wenting Wu^a, Qingshan Zhao^a, Han Hu^a, Yan Song^b, Mingbo Wu^{a,*}

^aState Key Laboratory of Heavy Oil Processing, Institute of New Energy, College of Chemical Engineering, China University of Petroleum (East China), Qingdao 266580, China

^bCAS Key Laboratory of Carbon Materials, Institute of Coal Chemistry, Chinese Academy of Sciences, Taiyuan 030001, China

*Corresponding author. Email: wumb@upc.edu.cn (M.B. Wu); ninghui@upc.edu.cn (H. Ning);
Tel.: +86-532-86983452.

Abstract

Electroreduction CO₂ to high value-added chemicals is a promising way to mitigate the greenhouse effect while storing the renewable electricity in chemicals. As an important chemical, C₂H₄ is a desirable product of CO₂ reduction but limited by lacking of efficient and durable catalysts. Herein, we proposed an interface-induced method to prepare Cu₂O nanocubes with controllable morphology and size. Due to the imidazolyl groups connected to the surface of ionic liquid functionalized graphite sheets (ILGS), Cu₂O nanocubes were induced to grow on ILGS to obtain Cu₂O/ILGS composites, where the size of Cu₂O can be controlled by adjusting the concentration of Cu²⁺. Interestingly, as the concentration of Cu²⁺ increases from 12.5 mmol/L to 100 mmol/L, the size of Cu₂O nanocubes decreases from 456 nm to 72 nm. As catalyst for CO₂ electroreduction in 0.1 M KHCO₃ aqueous solution, Cu₂O/ILGS-100 (synthesized under 100 mmol/L CuCl₂) behaves the best catalysis performance with a high faradic efficiency of C₂H₄ (31.1%) and long durability at -1.15 V (vs. reversible hydrogen electrode).

Key words:

CO₂ electroreduction; graphite sheets; ionic liquid; ethylene; cuprous oxide

1. Introduction

Electroreduction of carbon dioxide (CO₂RR) to high value-added chemicals offers an opportunity for alleviating the greenhouse effect and storing the renewable electricity in chemicals [1-4]. Recent progresses in electroreduction of CO₂ mainly focus on the production of gaseous carbon products, such as carbon monoxide (CO) [5, 6] methane (CH₄) [7, 8] and ethylene (C₂H₄) [9, 10], of which C₂H₄ is of significant value but limited by lacking of efficient and durable catalysts [11].

Among all the screened materials, copper-based materials have shown the best performance for electrocatalytic CO₂ to hydrocarbons, especially for C₂H₄ [12-15]. Recently, Cu₂O is found to have high selectivity to C₂H₄ in electrocatalytic CO₂RR, whose performance is closely related to its morphology and size [16-20]. Recent research has proved that the surface of Cu₂O is reduced to Cu⁰ with O vacancies during the CO₂RR [21], which is greatly affected by the applied potentials and currents [22]. The high C₂H₄ selectivity brought by Cu₂O catalysts is more likely due to a high density of grain boundaries with plenty of unsaturated coordinated copper atom with suitable atomic spacing. Liu et al. [23] proposed a metal embedded in oxidized matrix model with quantum mechanics methods to explain the activity and selectivity of Cu₂O in electrocatalytic CO₂RR, indicating that the Cu₂O matrix plays the key role in maintaining the high performance of oxide derived Cu⁰.

As a result, construction of Cu₂O crystals with suitable morphology and size to exposure plenty of unsaturated coordinating Cu atoms are crucial to improving the activity and selectivity of Cu₂O for electrocatalytic CO₂RR to C₂H₄. Unfortunately, the synthesis of well-defined and highly dispersed Cu₂O nanocrystals is still a great challenge. Huang et al. prepared Cu₂O nanocubes by controlling the aggregation of Cu₂O seed particles and surface reconstruction method via sodium dodecyl sulfate as capping surfactant [24]. Yeo et al. reported copper(I) oxide films electrodeposited from an electrolyte of 0.3 mol/L CuSO₄, 3.2 mol/L NaOH and 2.3 mol/L Lactic acid in water at various electrochemical potentials [25]. Wang et al. prepared Cu₂O hollow spheres by adjusting the concentration of CTAB in water under 60 °C [26]. These reported methods usually need trivial steps and massive energy consumption, bulk organic solvents or mass surfactants, which are environmentally unfriendly. Therefore, it is of great significance to invent an economic method for controllable synthesis of Cu₂O nanocrystals with high catalytic performance for C₂H₄ production from CO₂RR.

The interface-induced method is an outstanding strategy for controllable preparation of metal materials [27]. Carbon materials generally possess excellent chemical and thermal stabilities, good electrical conductivity [28], and flexible designability, making them promising candidates as supports to synthesize metal based composites based on interface-induced method [29, 30]. Pan et al. developed a facile interface-induced Zn(II)-ligand-fragment co-assembly strategy to in situ fabricate boronate-based MOF membrane on hydrophobic porous carbon substrate for specific molecular recognition and separation. A catechol-containing medicinal natural flavone luteolin

was found to be efficiently and selectively recognized on the MOF composite in water-containing solution due to the phenylboronic acid groups and carbon substrate^[31]. Ren et al. employed the graphene oxide (GO) support to template Cu₂O nanocrystals resulting in well-dispersed Cu₂O nanocrystals that show much promise in photo and chemo-catalytic applications, where GO play roles as the template and a surfactant to achieve dispersed Cu₂O crystals^[32]. These preliminary works motivate us to investigate the interface-induced method with carbon materials for controllable synthesis of Cu₂O nanocubes as high efficient catalyst for ethylene production from CO₂RR.

Herein, the ionic liquid functionalized graphite sheets (ILGS) were prepared by electro-exfoliation method according to our previous works^[33], which was dispersed into aqueous solution to construct ILGS-water interface. Under the interface effects of ILGS on Cu²⁺, a series of well-defined Cu₂O nanocubes were in situ fabricated on the surface of ILGS, in which the morphology and size of Cu₂O were completely different with those without ILGS. The as-prepared Cu₂O/ILGS showed significant enhancement of catalytic performance for ethylene formation in CO₂RR.

2. Experiment

2.1 Materials

1-octyl-3-methylimidazolium chloride (OmimCl, 99.0%) was supplied from the Centre of Green Chemistry and Catalysis, LICP, CAS, P. R. China. Copper chloride dihydrate (99.0%), sodium hydroxide (96.0%), potassium hydrogen carbonate (99.5%), ethanol anhydrous (99.7%) and L-ascorbic acid (99.99%) are provided by Sinopharm Chemical Reagent Co., Ltd., P. R. China. Nafion N-117 membranes (0.180 mm thick, ≥ 0.90 meq·g⁻¹ exchange capacity) were purchased from Alfa Aesar China Co., Ltd. High purity graphite rod ($\phi = 3$ mm) was provided by Beijing Crystal Dragon Carbon Technology Co., Ltd., P. R. China. All the reagents are used as received without further treatments. The water was purified by a Millipore system in all experiments.

2.2 Synthesis of Cu₂O/ILGS

Cu₂O/ILGSs were prepared using a simple wet chemical approach. Firstly, ILGS was synthesized according to our previous work^[33]. Then, 40 mg ILGS is added into 40 mL water to obtain a well-dispersed suspension under ultrasonic for 30 min at room temperature, denoted as solution A. After that, 12 mL of 12.5 mmol/L CuCl₂ aqueous solution was mixed with solution A and stirred vigorously for 1 hour, flowing by adding 20 mL of 0.1 mol/L NaOH slowly under stirring to obtain solution B. Subsequently, 50 mL of 6 mmol/L L-ascorbic acid is added to solution B and stirred for 2 hours at room temperature. At last, the precipitate was filtered and washed with water and ethanol thoroughly before drying under vacuum at 60 °C for 6 hours to obtain a brown powder, denoted as Cu₂O/ILGS-12.5. Cu₂O/ILGS-25, Cu₂O/ILGS-50, and Cu₂O/ILGS-100 were prepared with the same procedure except that the concentration of CuCl₂ is 25, 50 and 100 mmol/L, respectively. The yields of synthesis method, the nominal and real amount of Cu₂O obtained with the method were listed in Table S1.

As control experiments, pristine Cu₂O-12.5, Cu₂O-25, Cu₂O-50 and Cu₂O-100 were also prepared with the same procedure without adding ILGS in solution A, where the number after the Cu₂O represented the concentration of Cu²⁺ (mmol/L).

2.3 Materials Characterization

The morphologies of materials were characterized by scanning electron microscopy (SEM, Hitachi S-4800, Japan). The crystal property and phase composition of all as-prepared materials were investigated by X-ray diffraction (X'Pert PRO MPD, Holland) with Cu K α radiation at 40 kV and 40 mA with Cu K α radiation ($\lambda=1.5406\text{\AA}$). The surface elemental compositions were recorded by X-ray photoelectron spectroscopy (XPS, Thermo Scientific Escalab 250XI, America) with Al K α radiation. UV-Vis absorption spectra were measured by a UV-Vis spectrophotometer (UV-2700, SHIMADZU). Thermogravimetric analysis (TGA) was carried on a Shimadzu TA-60Ws thermal analyser (Japan) in air at a ramp rate of 10 °C min⁻¹.

2.4 CO₂RR and product analysis

The CO₂RR was carried out in an H-type electrolytic cell with two compartments, where the anode and cathode were separated by a Nafion 117 proton exchange membrane. A Pt plate (1×1 cm²) and Ag/AgCl electrode (KCl saturated) were used as counter and reference electrode, respectively. Both compartments were filled with 30 mL of 0.1 M KHCO₃ as electrolyte. All the working potentials were referred to the reversible hydrogen electrode (RHE). The pH value of the CO₂ saturated electrolyte is 6.8. All the electrochemical measurements were performed using an electrochemical workstation (CHI 760, Shanghai CH Instruments Co., P. R. China).

The working electrode was fabricated by drop-casting 100 μ L of catalyst ink onto a L-type glassy-carbon (GC, $\phi = 10$ mm) and dried with N₂. Before ink deposition, the GC electrode was polished and sonicated in ethanol. The catalyst inks were prepared by dispersing 5.0 mg materials in 10 μ L of 5% Nafion solution and 500 μ L of ethanol anhydrous.

Before testing, the electrolyte in cathode side was saturated with N₂ for 30 min to exclude air. Then high purity CO₂ (99.999%) was bubbled into the electrolyte for another 30 min. During the electrochemical measurements, the CO₂ gas flow was controlled at 20 mL/min. The gas-phase products generated during CO₂ electrolysis at each fixed potential were collected and quantitatively analyzed by gas chromatograph (BFRL-3420A, China), which was online connected with the head space of the cathodic side of the H-type cell. The gas products were injected to GC using a ten-port valve system with high purity Ar (99.999%) as carrier gas. The GC system was equipped with two columns associating with two detectors. The thermal conductivity detector (TCD) was installed to detect hydrogen and carbon monoxide while the flame ionization detector (FID) was fabricated to detect hydrocarbons. The liquid product was tested with Nash's colorimetric method by UV-Vis spectrophotometer^[35]. The faradaic efficiency of all products was calculated according to the methods reported by Yeo et al^[25].

3. Results and Discussion

The typical preparation procedure is schematically illustrated in Scheme 1. The XRD patterns

(Fig. 1) and XPS spectra (Fig. 2) indicate that Cu₂O nanocrystals are successfully synthesized and in-situ supported on the ILGS. As shown in Fig. 1, the wider diffraction peak at 26.43° is ascribed to the (002) peak of ILGS due to the increased amorphousness and defects after exfoliation of graphite. Other diffraction peaks can be exactly indexed to Cu₂O (JCPDS No.78-2076) at 29.58° (110), 36.44° (111), 42.33° (200), 52.49° (211), 61.40° (220), and 73.56° (311), respectively. No other characteristic peaks exist in the XRD patterns, indicating Cu₂O was successfully synthesized and in-situ supported on ILGS.

It can be seen from the XPS spectra (Fig. 2a) that all Cu₂O/ILGSs consist of C, N, O and Cu. In Fig. 2b, the peaks at 399.57 eV and 401.06 eV indicate that nitrogen in ILGS is derived from the cations of 1-octyl-3-methylimidazolium chloride, which is used as electrolyte for graphite electro-exfoliation^[36]. In Fig. 2c, the characteristic peaks at 932.1 eV and 952.0 eV are corresponding to Cu2p_{3/2} and Cu2p_{1/2}, respectively. The specific valence of Cu⁺ and Cu⁰ was further investigated by Cu LMM Auger spectra (Fig. 2d), the kinetic energy around 916.9 eV confirms the purity of Cu₂O without Cu⁰ existing^[37].

SEM images revealed that all the Cu₂O nanocrystals present cubic morphology with obviously different size distributions, as shown in Fig. 3 and Fig. S1. To be specific, obvious cavities on the surface of Cu₂O nanocubes were found in Cu₂O/ILGS-12.5 due to incomplete growing, which is beneficial for the exposure of unsaturated coordinate Cu atoms. The size distribution of Cu₂O nanocubes supported on ILGS showed an abnormal rule in comparison with pristine Cu₂O. As shown in Fig. S2 and Table S2, with the concentration of Cu²⁺ increasing from 12.5 mmol/L to 100 mmol/L, the average side length of Cu₂O in Cu₂O/ILGSs decreases from 456 nm to 72 nm, while the average side length of pristine Cu₂O increases from 113 nm to 228 nm, indicating the ILGS can inhibit the growth and aggregation of Cu₂O crystals under high concentration of Cu²⁺.

The catalytic performances of Cu₂O/ILGSs for CO₂ electroreduction to C₂H₄ were investigated with CO₂-saturated 0.1 M KHCO₃ solution as electrolyte in an H-type cell under series potentials. The faradaic efficiency of C₂H₄ and other gas products were depicted in Fig. 4. For all Cu₂O/ILGSs, the optimum values of faradaic efficiency for C₂H₄ are at -1.15 V (vs. RHE). Cu₂O/ILGS-100 shows a maximum faradaic efficiency (FE) of 31.1% for C₂H₄ products. As shown in Fig. S3, formate as the only liquid product was detected with a combined FE of ca. 100% with gas products for Cu₂O/ILGS-100.

In our previous work, ILGS has been proved to have no catalytic activity for electroreduction of CO₂ while Cu₂O is the main active sites. For pristine Cu₂O (Fig. 4e), along with the average size of Cu₂O increasing from 113 nm to 228 nm, the FE_{C₂H₄} declines from 17.5% to 13.8%. Similar trends can also be found for Cu₂O/ILGS-25, Cu₂O/ILGS-50 and Cu₂O/ILGS-100. Reasonably, the highest FE_{C₂H₄} (31.1 %) was obtained over Cu₂O/ILGS-100 due to the smallest size of Cu₂O nanocubes (72 nm). Specially, the FE of C₂H₄ on Cu₂O/ILGS-12.5 is 25.5%, which is close to Cu₂O/ILGS-25 (25.0%), though the size of Cu₂O in Cu₂O/ILGS-12.5 is much larger than that in Cu₂O/ILGS-25. This special phenomenon is corresponding to the special morphology

of Cu₂O with obviously cavities on the crystal surface (Fig. 3a), which may arise from the interface-induced effects of ILGS associating with the low concentration of Cu²⁺. These concavities increase the density of grain boundaries of Cu₂O nanocubes with more unsaturated copper atoms exposed, which is conducive to enhancing the selectivity of C₂H₄ [38]. Among all the materials as made, the Cu₂O nanocubes in Cu₂O/ILGS-100 have the largest loading of 77.6 wt% (Fig. S4, Table S3) and the smallest size of 72 nm, indicating this is a facile method for rapid synthesis of smaller Cu₂O nanocubes using high concentrations of Cu²⁺ for industrial applications.

It is worth noting the mass activity of Cu₂O towards ethylene formation is meaningful for evaluating the real catalytic activity of copper. Under the optimum potential -1.15V (*vs.* RHE), the formation rate of ethylene on unit mass of Cu₂O was calculated, as shown in Fig. S5. Not surprisingly, Cu₂O/ILGS-12.5 presents the best performance due to its lowest loading of Cu₂O with obvious concavities, flowing by Cu₂O/ILGS-25 and Cu₂O/ILGS-50. Interestingly, Cu₂O/ILGS-100 exits a relative high yield of C₂H₄, much better than Cu₂O/ILGS-50 and Cu₂O/ILGS-25, with the highest Cu₂O loading. With further to explain this phenomenon, the BET surface area of different materials as-made was calculated according to N₂ adsorption-desorption isotherms. As depicted in Fig. S6, the BET surface area of Cu₂O/ILGS-12.5, Cu₂O/ILGS-25, Cu₂O/ILGS-50 and Cu₂O/ILGS-100 is 5.90, 5.23, 6.07, and 6.30 m² g⁻¹, respectively, which is closely related to the size and morphology of Cu₂O nanoparticles. Cu₂O/ILGS-100 has the largest specific surface area due to its smallest size of Cu₂O crystals. However, Cu₂O/ILGS-12.5 has a larger specific surface area than Cu₂O/ILGS-25, even though the latter has a much smaller size of Cu₂O. This is consistent with the special morphology of Cu₂O crystals in Cu₂O/ILGS-12.5, which have obvious surface cavities (Fig. 3a). As revealed by the linear sweep voltammetry (LSV) curve in Fig. S7a, Cu₂O/ILGS-100 achieved the highest total current density from -0.85 V to -1.3 V (*vs.* RHE). According to the mass content of Cu supported on ILGS, the mass-specific current density of all the catalysts was tested and normalized by 1.0 mg copper, as shown in Fig. S7b. It is found that Cu₂O/ILGS-100 still has the largest current density under the measured potentials, indicating that ILGS as supports facilitate the utilization of Cu atom as catalyst for CO₂ electroreduction.

In the end, the stabilities of Cu₂O/ILGS-100 and Cu₂O/ILGS-12.5 were selected as representative samples to investigated the durability of Cu₂O under -1.15 V (*vs.* RHE), as depicted in Fig. 4f and Fig. S8, respectively. Despite the great difference of Cu₂O nanocubes in size and morphology, both Cu₂O/ILGS-100 and Cu₂O/ILGS-12.5 showed better durability than the corresponding pristine Cu₂O, indicating the interface-induced method is preferable to synthesize Cu₂O materials with higher selectivity and better durability for electrocatalytic reduction of CO₂ towards C₂H₄. We further explored the morphology and state of Cu₂O after CO₂ electroreduction. Taking Cu₂O/ILGS-100 for example, the edge of Cu₂O nanocubes is blurred (Fig. S9), indicating the morphology of Cu₂O is not stable during the CO₂ electroreduction [39]. As shown in Fig. S10, the Cu 2p XPS showed that Cu⁺ or Cu⁰ exists in Cu₂O/ILGS-100 and no Cu²⁺ peaks were observed. With further analyzed from the Auger Cu LMM line (Fig. S11), it is concluded that only minimal Cu⁺ was reduced to Cu⁰ under the applied negative potential and Cu⁺ is still the main

active species in Cu₂O/ILGS-100, which play the key role in selectively catalytic CO₂RR to ethylene^[19].

4. Conclusions

In summary, an interface-induced method was developed to synthesize Cu₂O nanocubes with controllable morphology and size. Due to the nanostructured surface functionalities of ILGS, Cu₂O nanocubes with smaller size and high loading amount on ILGS were prepared. As the concentration of Cu²⁺ decreases from 100 mmol/L to 12.5 mmol/L, the size of Cu₂O on ILGS increases from 72 nm to 456 nm, while the size of pristine Cu₂O without ILGS as supports decreases from 228 nm to 113 nm. This abnormal phenomenon was ascribed to the interface effects of ILGS: (1) The Cu₂O nucleus is preferable to generate on the surface of ILGS rather than in the bulk solution due to the absorption effect of ILGS to Cu²⁺; (2) The nanostructures of ILGS can fix the position of Cu₂O crystals and inhibit their aggregation. Under the optimal potential for C₂H₄ formation (-1.15 V vs. RHE), all Cu₂O/ILGSs show higher selectivity towards C₂H₄ than the corresponding pristine Cu₂O prepared with the same concentration of Cu²⁺, of which Cu₂O/ILGS-100 exhibits the highest faradic efficiency of ethylene (31.1%). The high performance of Cu₂O/ILGS-100 is attributed to its larger electrochemically active surface area than Cu₂O/ILGS-50, Cu₂O/ILGS-12.5 and Cu₂O/ILGS-25. It is worth noting that Cu₂O nanocubes in Cu₂O/ILGS-100 present the smallest size of 72 nm and the highest loading amount of 77.6 wt%, indicating this interface-induced method has a great potential in scaling up synthesis of small size of Cu₂O with high concentrations of Cu²⁺. This work not only paves the way for scale preparation of well-defined Cu₂O nanocubes as efficient catalyst for green synthesis of ethylene from CO₂RR, but also enlightens a facile way to control the morphology and size of metal oxides for various electrochemical applications.

Acknowledgements

This work is financially supported by the National Natural Science Foundation of China (Nos. 21808242, 51572296); the Natural Science Foundation of Shandong Province (ZR2018BB070), the Financial Support from Taishan Scholar Project.

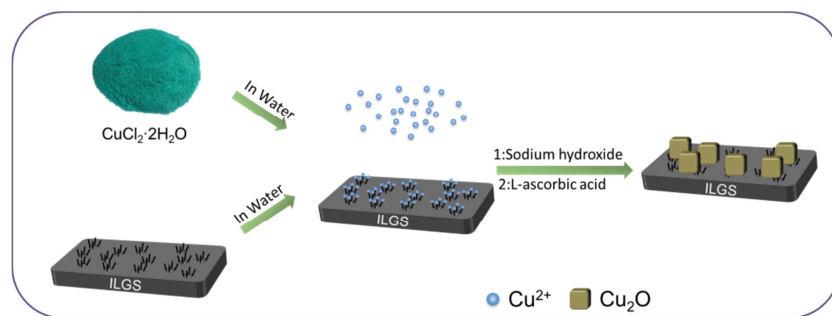
References

- [1] M. He, Y. Sun, B. Han, Green carbon science: scientific basis for integrating carbon resource processing, utilization, and recycling, *Angew. Chem. Int. Ed.* 52 (2013) 9620-9633.
- [2] X. Chang, T. Wang, J. Gong, CO₂ photo-reduction: insights into CO₂ activation and reaction on surfaces of photocatalysts, *Energy Environ. Sci.* 9 (2016) 2177-2196.
- [3] Y. Wang, J. Liu, Y. Wang, A.M. Al-Enizi, G. Zheng, Tuning of CO₂ Reduction Selectivity on Metal Electrocatalysts, *Small*, 13 (2017) 1701809.
- [4] A. Vasileff, C. Xu, Y. Jiao, Y. Zheng, S.-Z. Qiao, Surface and Interface Engineering in Copper-Based Bimetallic Materials for Selective CO₂ Electroreduction, *Chem*, 4 (2018)

- 1809-1831.
- [5] F. Li, M. Xue, G. P. Knowles, L. Chen, D. R. MacFarlane, J. Zhang, Porous nitrogen-doped carbon derived from biomass for electrocatalytic reduction of CO₂ to CO, *Electrochim. Acta* 245 (2017) 561-568.
- [6] L. Jin, B. Liu, P. Wang, H. Yao, L.A. Achola, P. Kerns, A. Lopes, Y. Yang, J. Ho, A. Moewes, Y. Pei, J. He, Ultrasmall Au nanocatalysts supported on nitrated carbon for electrocatalytic CO₂ reduction: the role of the carbon support in high selectivity, *Nanoscale* 10 (2018) 14678-14686.
- [7] X. Liu, H. Yang, J. He, H. Liu, L. Song, L. Li, J. Luo, Highly Active, Durable Ultrathin MoTe₂ Layers for the Electroreduction of CO₂ to CH₄, *Small* 14 (2018) 1704049.
- [8] X. Sun, X. Kang, Q. Zhu, J. Ma, G. Yang, Z. Liu, B. Han, Very highly efficient reduction of CO₂ to CH₄ using metal-free N-doped carbon electrodes, *Chem. Sci.* 7 (2016) 2883-2887.
- [9] A. Loiudice, P. Lobaccaro, E. A. Kamali, T. Thao, B. H. Huang, J. W. Ager, R. Buonsanti, Tailoring Copper Nanocrystals towards C₂ Products in Electrochemical CO₂ Reduction, *Angew. Chem. Int. Ed.* 128 (2016) 5883-5886.
- [10] D. Wu, C. Dong, D. Wu, J. Fu, H. Liu, S. Hu, Z. Jiang, S.-Z. Qiao, X.-W. Du, Cuprous ions embedded in ceria lattice for selective and stable electrochemical reduction of carbon dioxide to ethylene, *J. Mater. Chem. A* 6 (2018) 9373-9377.
- [11] F. S. Roberts, K. P. Kuhl, A. Nilsson, High Selectivity for Ethylene from Carbon Dioxide Reduction over Copper Nanocube Electrocatalysts, *Angew. Chem. Int. Ed.* 54 (2015) 5179-5182.
- [12] H. Xie, T. Wang, J. Liang, Q. Li, S. Sun, Cu-based nanocatalysts for electrochemical reduction of CO₂, *Nano Today* 21 (2018) 41-54.
- [13] Y. Hori, K. Kikuchi, S. Suzuki, Production of CO and CH₄ in electrochemical reduction of CO₂ at metal electrodes in aqueous hydrogen carbonate solution, *Chem. Lett.* 14 (1985) 1695-1698.
- [14] Y. Jiao, Y. Zheng, P. Chen, M. Jaroniec, S. Qiao, Molecular scaffolding strategy with synergistic active centers to facilitate electrocatalytic CO₂ reduction to hydrocarbon/alcohol, *J. Am. Chem. Soc.* 139 (2017) 18093-18100.
- [15] C.F.C. Lim, D.A. Harrington, A.T. Marshall, Effects of mass transfer on the electrocatalytic CO₂ reduction on Cu, *Electrochim. Acta* 238 (2017) 56-67.
- [16] C. W. Lee, K. D. Yang, D. H. Nam, J. H. Jang, N. H. Cho, S. W. Im, K. T. Nam, Defining a materials database for the design of copper binary alloy catalysts for electrochemical CO₂ conversion, *Adv. Mater.* 30 (2018) 1704717.
- [17] P. D. Luna, R. Quintero-Bermudez, C. Dinh, M. B. Ross, O. S. Bushuyev, P. Todorović, T. Regier, S. O. Kelley, P. Yang, E. H. Sargent, Catalyst electro-redeposition controls morphology and oxidation state for selective carbon dioxide reduction, *Nat. Catal.* 1 (2018) 103-110.
- [18] Y. Chen, C. W. Li, M. W. Kanan, Aqueous CO₂ reduction at very low overpotential on oxide-derived Au nanoparticles, *J. Am. Chem. Soc.* 134 (2012) 19969-19972.
- [19] C. Chen, X. Sun, L. Lu, D. Yang, J. Ma, Q. Zhu, Q. Qian, B. Han, Efficient electroreduction of CO₂ to C₂ products over B-doped oxide-derived copper, *Green Chem.* 20 (2018) 4579-4583.
- [20] A. Eilert, F. Cavalca, F. S. Roberts, J. Osterwalder, C. Liu, M. Favaro, E.J. Crumlin, H.

- Ogasawara, D. Friebel, L. G. Pettersson, A. Nilsson, Subsurface oxygen in oxide-derived copper electrocatalysts for carbon dioxide reduction, *J. Phys. Chem. Lett.* 8 (2017) 285-290.
- [21] Y. Lum, J. W. Ager, Stability of residual oxides in oxide-derived copper catalysts for electrochemical CO₂ reduction investigated with ¹⁸O labeling, *Angew. Chem. Int. Ed.* 57 (2018) 551-554.
- [22] D. Ren, J. Fong, B. S. Yeo, The effects of currents and potentials on the selectivities of copper toward carbon dioxide electroreduction, *Nat. Commun.* 9 (2018) 925.
- [23] D. Kim, C. S. Kley, Y. Li, P. Yang, Copper nanoparticle ensembles for selective electroreduction of CO₂ to C₂-C₃ products, *PNAS* 114 (2017) 10560-10565.
- [24] C. H. Kuo, C. H. Chen, M. H. Huang, Seed-Mediated Synthesis of Monodispersed Cu₂O Nanocubes with Five Different Size Ranges from 40 to 420 nm, *Adv. Funct. Mater.* 17 (2007) 3773-3780.
- [25] D. Ren, Y. Deng, A. D. Handoko, C. S. Chen, S. Malkhandi, B. S. Yeo, Selective electrochemical reduction of carbon dioxide to ethylene and ethanol on copper(i) oxide catalysts, *ACS Catal* 5 (2015) 2814-2821.
- [26] H. Xu, W. Wang, Template synthesis of multishelled Cu₂O hollow spheres with a single-crystalline shell wall, *Angew. Chem. Int. Ed.* 46 (2007) 1489-1492.
- [27] Z. Zuo, Y. Wen, S. Zhang, Interface-induced nucleation and growth: a new route for fabricating ordered silver nanohole arrays, *Nanoscale* 10 (2018) 14039-14046.
- [28] M. Ding, F. Du, B. Liu, Z. Y. Leong, L. Guo, F. Chen, A. Baji, H. Y. Yang, Rod-like nitrogen-doped carbon hollow shells for enhanced capacitive deionization, *FlatChem*, 7 (2018) 10-17.
- [29] J. Yuan, W. Zhi, L. Liu, M. Yang, H. Wang, J. Lu, Electrochemical reduction of CO₂ at metal-free N-functionalized graphene oxide electrodes, *Electrochim. Acta* 282 (2018) 694-701.
- [30] L. Qu, Y. Liu, J. Baek, L. Dai, Nitrogen-doped graphene as efficient metal-free electrocatalyst for oxygen reduction in fuel cells, *ACS nano* 4 (2010) 1321-1326.
- [31] S. Liu, S. Shinde, J. Pan, Y. Ma, Y. Yan, G. Pan, Interface-induced growth of boronate-based metal-organic framework membrane on porous carbon substrate for aqueous phase molecular recognition, *Chem. Eng. J* 324 (2017) 216-227.
- [32] C. Hong, X. Jin, J. Totleben, J. Lohrman, E. Harak, B. Subramaniam, R. V. Chaudharib, S. Ren, Graphene oxide stabilized Cu₂O for shape selective nanocatalysis, *J. Mater. Chem. A* 2 (2014) 7147-7151.
- [33] H. Ning, W. Wang, Q. Mao, S. Zheng, Z. Yang, Q. Zhao, M. Wu, Catalytic electroreduction of CO₂ to C₂H₄ using Cu₂O supported on 1-Octyl-3-methylimidazole functionalized graphite sheets, *Acta Phys. -Chim. Sin.* 34 (2018) 938-944.
- [34] T. T. Zhuang, Z. Q. Liang, A. Seifitokaldani, Y. Li, P. D. Luna, T. Burdyny, F. Che, F. Meng, Y. Min, R. Quintero-Bermudez, C. T. Dinh, Y. Pang, M. Zhong, B. Zhang, J. Li, P. N. Chen, X. L. Zheng, H. Liang, W. N. Ge, B. J. Ye, D. Sinton, S. H. Yu, E. H. Sargent, Steering post-C-C coupling selectivity enables high efficiency electroreduction of carbon dioxide to multi-carbon alcohols, *Nature Catal.* 1 (2018) 421-428.
- [35] J. Hong, W. Zhang, J. Ren, R. Xu, Photocatalytic reduction of CO₂: a brief review on product analysis and systematic methods, *Anal. Methods* 5 (2013) 1086.
- [36] N. Liu, F. Luo, H. Wu, Y. Liu, C. Zhang, J. Chen, One-step ionic-liquid-assisted

- electrochemical synthesis of ionic-liquid-functionalized graphene sheets directly from graphite, *Adv. Funct. Mater.* 18 (2008) 1518-1525.
- [37] S. Y. Lee, H. Jung, N. K. Kim, H. S. Oh, B. K. Min, Y. J. Hwang, Mixed copper states in anodized Cu electrocatalyst for stable and selective ethylene production from CO₂ Reduction, *J. Am. Chem. Soc.* 140 (2018) 8681-8689.
- [38] Y. Huo, X. Peng, X. Liu, H. Li, J. Luo, High selectivity toward C₂H₄ production over Cu particles supported by butterfly-wing-derived carbon frameworks, *ACS Appl. Mater. Interfaces* 10 (2018) 12618-12625.
- [39] P. Grosse, D. Gao, F. Scholten, I. Sinev, H. Mistry, B. Roldan Cuenya, Dynamic Changes in the Structure, Chemical State and Catalytic Selectivity of Cu Nanocubes during CO₂ Electroreduction: Size and Support Effects, *Angew. Chem. Int. Ed.* 57 (2018) 6192-6197.



Scheme. 1 Illustration for preparation of Cu₂O/ILGS.

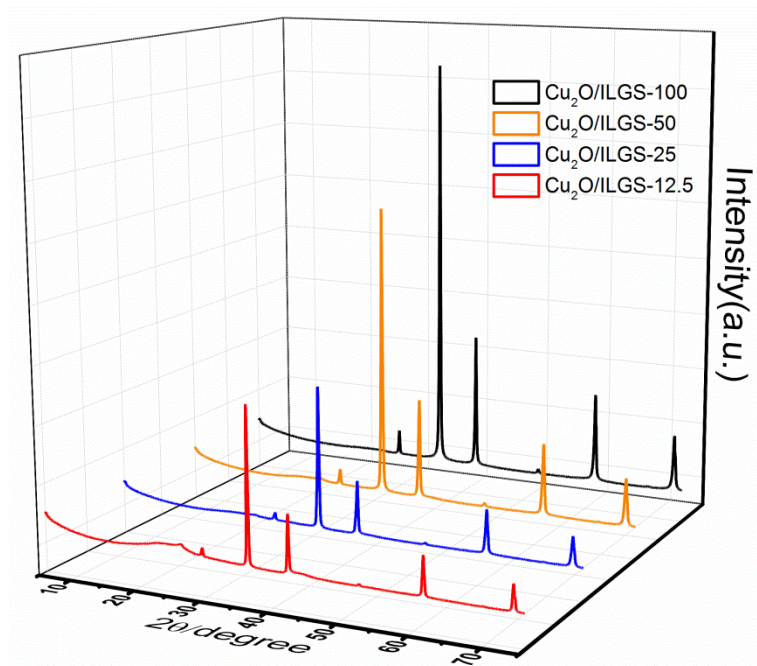


Fig. 1 XRD patterns of Cu₂O/ILGSs.

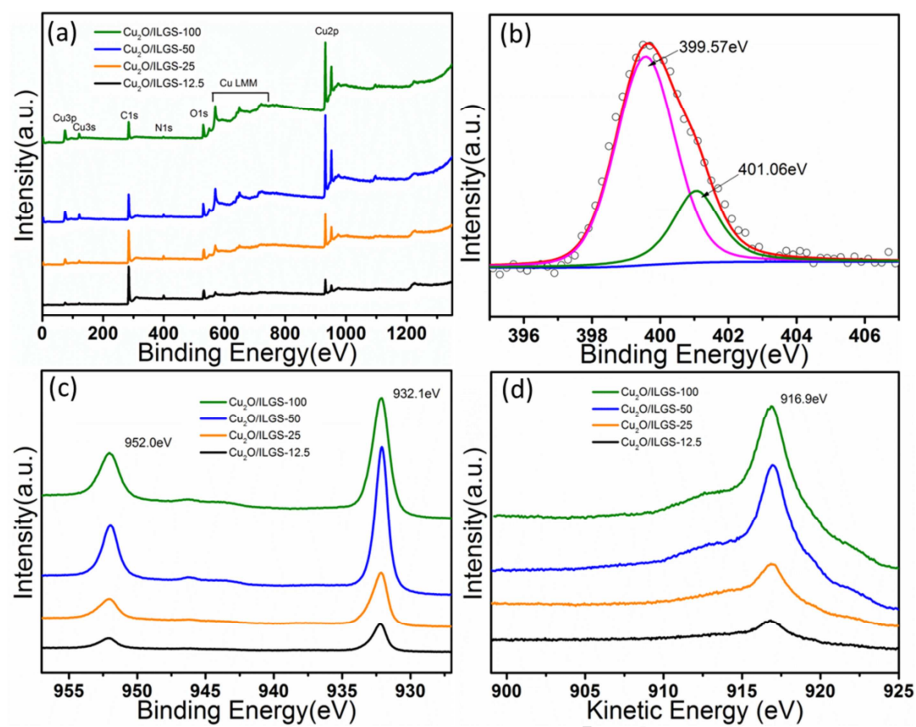


Fig. 2 (a) XPS spectra of Cu₂O/ILGSs, (b) High-resolution N1s spectra of Cu₂O/ILGS-12.5, (c) High-resolution Cu2p spectra of Cu₂O/ILGSs, (d) Cu LMM Auger spectra of Cu₂O/ILGSs.

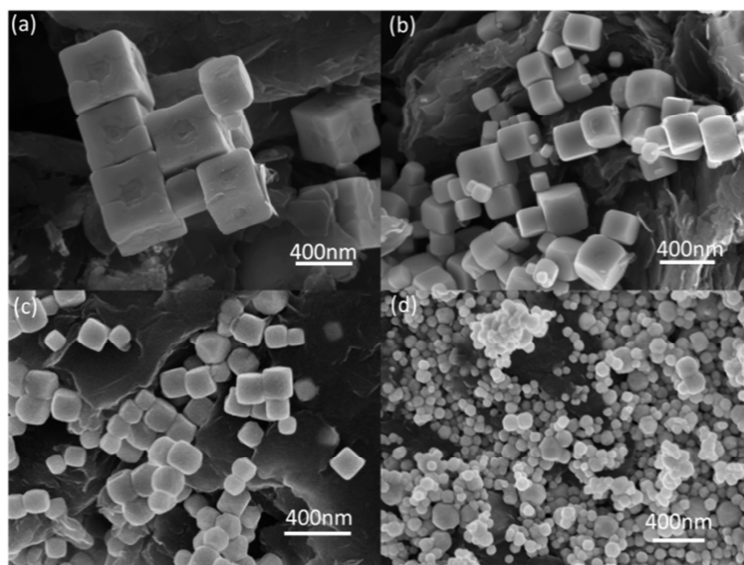


Fig. 3 SEM images of (a) Cu₂O/ILGS-12.5, (b) Cu₂O/ILGS-25, (c) Cu₂O/ILGS-50, (d) Cu₂O/ILGS-100.

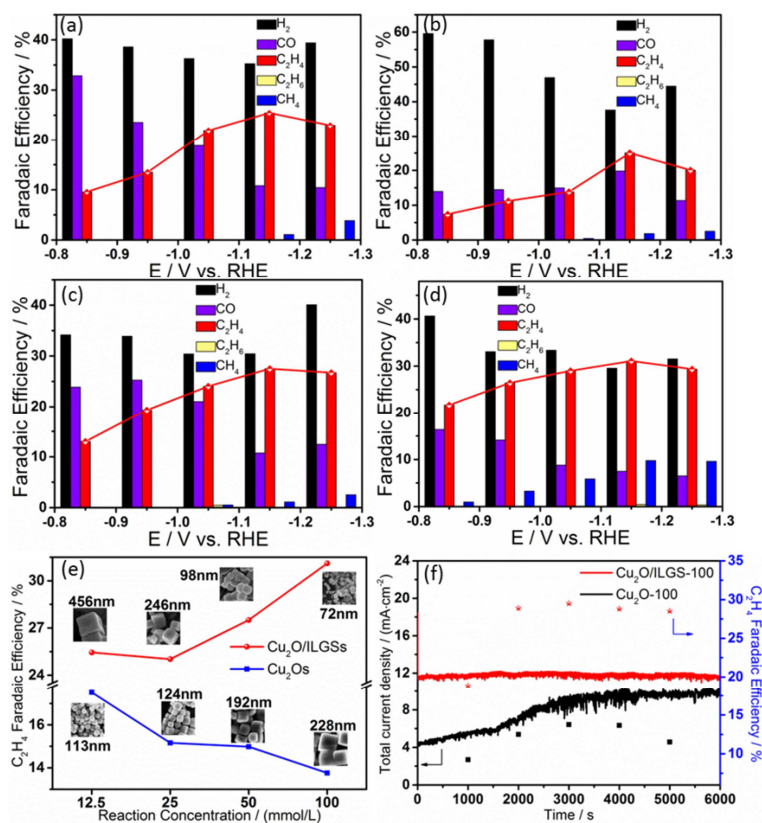


Fig. 4 Faradaic efficiencies of gas products from CO₂RR on (a) Cu₂O/ILGS-12.5, (b) Cu₂O/ILGS-25, (c) Cu₂O/ILGS-50, (d) Cu₂O/ILGS-100. (e) Comparison of FE_{C₂H₄} on Cu₂O/ILGSs and Cu₂O_s at -1.15 V (vs. RHE). The insets illustrate the morphology and size of Cu₂O. (f) Stability test of Cu₂O/ILGS-100 and Cu₂O-100 at -1.15 V (vs. RHE).